

Boosting photoelectrocatalytic oxygen evolution activity of BiVO₄ photoanodes via caffeic acid bridged to NiFeOOH

Xiaohu Li^a, Junhao Wu^a, Congzhao Dong^a, Yao Kou^a, Chunlian Hu^a, Jinnuo Zang^a, Jiayu Zhu^a, Baochun Ma^a, Yuanyuan Li^c, Yong Ding^{a,b,*}

^a State Key Laboratory of Applied Organic Chemistry, Key Laboratory of Advanced Catalysis of Gansu Province, College of Chemistry and Chemical Engineering, Lanzhou University, Lanzhou 730000, China

^b State Key Laboratory of Low Carbon Catalysis and Carbon Dioxide Utilization; State Key Laboratory for Oxo Synthesis and Selective Oxidation, Lanzhou Institute of Chemical Physics, Chinese Academy of Sciences, Lanzhou 730000, China

^c Department of Biological and Chemical Engineering, Chongqing University of Education, Chongqing 400067, China



ARTICLE INFO

Keywords:

Photoelectrochemical reaction
Water splitting
Bismuth vanadate
Caffeic acid
Oxygen evolution

ABSTRACT

Bismuth vanadate (BiVO₄) is a promising n-type photoanode material for photoelectrochemical (PEC) water splitting. However, its activity is impeded by poor charge carrier transport and sluggish oxygen evolution kinetics. In this study, we report a Fe doping and caffeic acid (CA)/NiFeOOH (NiFe) modification with BiVO₄ photoanode (NiFe/CA/Fe-BiVO₄) to enhance the PEC water oxidation performance and stability. The modified BiVO₄ demonstrates significant advantages in promoting the PEC performance and stability. Specifically, Fe doping via in-situ electro-deposition results in smaller crystal sizes, larger specific surface areas, and more exposed active sites. Furthermore, co-catalyst NiFe connects with Fe-BiVO₄ through CA bridge facilitates a more uniform self-assembly distribution of NiFe on BiVO₄ surface. The NiFe/CA/Fe-BiVO₄ exhibits an excellent photocurrent density of 6.2 mA/cm² at 1.23 V_{RHE} and demonstrates good stability at 0.8 V_{RHE}. In addition, the composite photoanode shows a high applied bias photon-to-current efficiency (ABPE) value of 2.15% at 0.65 V_{RHE}. EPR and in-situ FTIR confirm the generation of superoxide active species (O₂ and ·O₂) during the PEC water oxidation reaction.

1. Introduction

Converting solar energy into clean hydrogen fuels via photoelectrochemical (PEC) water splitting has been considered as a highly promising and effective strategy [1–3]. Due to the narrow bandgap (2.4 eV) and suitable energy-band position [4,5], BiVO₄ is regarded as a highly potential photoanode material for overcoming the slow water oxidation half-reaction (OER) kinetics [6,7]. However, the easy recombination of charge carriers in BiVO₄ and its slow surface dynamics result in the majority of photo-generated carriers recombining in the bulk and at the surface, which hinder BiVO₄ from reaching its theoretical maximum photocurrent density (7.5 mA/cm², AM 1.5 G, 100 mW/cm²) at 1.23 V_{RHE} [8–10]. Meanwhile, V⁵⁺ dissolution from the crystal under illumination causes the photocurrent of the BiVO₄ photoanode to drop significantly within a short period of time [11]. Therefore, it is crucial for BiVO₄ to enhance the PEC performance and

improve the long-time stability. Various strategies, such as morphology engineering [12,13], elemental doping [14–16], surface facet control [17–19], constructing heterojunctions [20], loading hole-transporting layers [21,22] and loading co-catalysts [23,24] have been developed, which are able to efficiently promote carrier separation and transport in the bulk phase and on the surface as well as to significantly improve the stability of BiVO₄.

The photocurrent density is significantly improved by doping BiVO₄ with heteroatom such as Mo, W, P, N and F [20,25–29]. In the past decade, transition metal oxides and hydroxides (such as FeOOH, NiOOH, NiOOH/FeOOH, NiFeOOH (NiFe), N:NiFeO_x and FeNiPO_x) on BiVO₄ as oxygen evolution co-catalysts (OEC) has been widely applied to enhance its PEC performance and stability [4,8,24,30–32]. Furthermore, some solution treatment methods have also been shown to significantly improve the PEC performance and stability of BiVO₄ [9,11,31,33]. For example, long-term photo-assisted electrochemical

* Corresponding author at: State Key Laboratory of Applied Organic Chemistry, Key Laboratory of Advanced Catalysis of Gansu Province, College of Chemistry and Chemical Engineering, Lanzhou University, Lanzhou 730000, China.

E-mail address: dingyong1@lzu.edu.cn (Y. Ding).

passivation of the BiVO_4 surface can greatly enhance its PEC performance and stability [33]. Simultaneously, the addition of V^{5+} to the reaction solution can effectively improve the stability of BiVO_4 [11]. Although there have been many reports to enhance the PEC performance of BiVO_4 via doping heteroatom, these methods are relatively expensive, and the study of interface relationships is still unclear.

Herein we reported a method for preparing a layer-by-layer structure NiFe/CA/Fe-BiVO_4 photoanode via doping in-situ electrochemical deposition process and with coffee acid (CA) as a coordinating-assisted impregnation agent. During the rapid formation of BiOI in electrodeposition, Fe is encapsulated into the lattice as a heteroatom. Experimental and characterization results demonstrated that the Fe was uniformly distributed in BiVO_4 , which improved the transport of photogenerated charge carriers at the bulk and surface, generated more oxygen vacancies, suppressed carrier recombination and enhanced water oxidation performance. Subsequently, coffee acid acted as a bridging agent to connect Fe-BiVO_4 and NiFe . Carboxyl groups at the end of coffee acid coordinated with Ni and Fe atoms, forming a uniform NiFeOOH outer layer during the impregnation process, which ultimately resulted in the layer-by-layer structure of NiFe/CA/Fe-BiVO_4 . This coordination-driven self-assembly process not only formed stable bonds for fast charge transfer but also provided a clear interface for structural-activity studies.

2. Materials and methods

The specific reagents, equipment, experimental procedures and analytical methods employed in this study are detailed in the [Supporting Information](#).

3. Results and discussion

3.1. Construction of NiFe/CA/Fe-BiVO_4 Photoanode

M-BiVO_4 ($\text{M} = \text{Fe, Co, Ni, Mn and Zn}$) was obtained based on a reported method with modification [8], which was prepared through doping in electrodeposition process and then high-temperature calcination. The doping elements and doping amounts had a significant impact on the performance of the photoanode. Different doping amounts of M-BiVO_4 were prepared by adding varying amounts of different chloride salts to the electrolyte. Among the five types of photoanodes doped with different heteroatoms, namely Fe-BiVO_4 , Co-BiVO_4 , Zn-BiVO_4 , Ni-BiVO_4 and Mn-BiVO_4 , the 0.5- Fe-BiVO_4 photoanode exhibit the highest photocurrent density, approximately 4.20 mA/cm^2 at $1.23 \text{ V}_{\text{RHE}}$ ([Fig. S1](#)). The elemental content of BiVO_4 and Fe-BiVO_4 are determined by inductively coupled plasma optical emission spectra (ICP-OES) ([Table S1](#)). Therefore, it was selected for subsequent studies.

After optimization doping concentrations, samples Ni-BiVO_4 , Co-BiVO_4 , Mn-BiVO_4 and Zn-BiVO_4 show the maximum photocurrent densities of 4.00 , 3.90 , 3.02 and 3.01 mA/cm^2 , respectively.

Scanning electron microscopy (SEM) is used for characterizing the morphology of photoanodes. BiVO_4 is uniformly grown on FTO with $200\text{--}400 \text{ nm}$ porous nanostructure ([Fig. 2a](#)). This structure is beneficial for enhancing the catalyst's light absorption, accelerating reactants diffusion and exposing more active sites. And Fe-BiVO_4 ([Fig. 2b](#)) exhibits a similar morphology to BiVO_4 . However, the nanoparticles of Fe-BiVO_4 are smaller than those of BiVO_4 , indicating that Fe doping alters the particle size of BiVO_4 and exposes more active sites. Fe doping takes place during the electrodeposition process of BiOI ([Fig. 1](#)). The presence of FeCl_3 in the solution results in a more negative current ([Fig. S2](#)). A more negative current will consume more H^+ , resulting in a more drastic change in pH near FTO [34], thus accelerating the crystallization process of BiOI and shortening the time required for crystallization. The faster crystallization process and shorter crystallization time results in the formation of smaller crystals. Because the particle size of BiOI decreased, crystal size of Fe-BiVO_4 became smaller than that of pure BiVO_4 . Subsequently, through the method of caffeic acid bridging and impregnation self-assembly, NiFeOOH co-catalyst was successfully constructed on Fe-BiVO_4 , resulting in the preparation of a NiFe/CA/Fe-BiVO_4 composite photoanode. It can be observed that the surface of Fe-BiVO_4 becomes noticeably rougher after loading NiFe/CA ([Fig. 2c](#)).

The transmission electron microscopy (TEM) spectra of BiVO_4 , Fe-BiVO_4 and NiFe/CA/Fe-BiVO_4 are shown in [Fig. S3](#), [S4](#) and [1d](#). Compared to BiVO_4 and Fe-BiVO_4 , NiFe/CA/Fe-BiVO_4 clearly exhibits a uniform outer layer of NiFe co-catalyst. The high-resolution transmission electron microscopy (HRTEM) image ([Fig. 2e](#)) also confirms the presence of the NiFe layer. In NiFe/CA/Fe-BiVO_4 , there is a NiFe film with a thickness of approximate 5 nm on the surface of Fe-BiVO_4 , and the interface between Fe-BiVO_4 and the NiFe layer is indicated by a yellow dashed line. The lattice fringe with a width of 0.237 nm corresponds to the (220) crystal plane of BiVO_4 . The homogeneous dispersion of Bi, V, O, Fe and Ni elements in samples are confirmed by the elemental mapping of NiFe/CA/Fe-BiVO_4 ([Fig. 2g](#)).

Additionally, crystal phase and crystallinity degree of BiVO_4 , Fe-BiVO_4 , CA/Fe-BiVO_4 and NiFe/CA/Fe-BiVO_4 samples are verified by the X-ray diffraction (XRD) patterns ([Fig. 2f](#)). It can be observed that all the diffraction peaks are attributed to monoclinic BiVO_4 (JCPDS No. 14-0688), suggesting that the doping does not alter the phase and crystallinity of BiVO_4 . However, no obvious diffraction peaks corresponding to NiFeOOH are detected in the XRD pattern, which is mainly due to its amorphous structure and ultra-thin thickness. Furthermore, the XRD patterns of other M-BiVO_4 ($\text{M} = \text{Co, Ni, Zn and Mn}$) are similar to BiVO_4 ([Fig. S5a](#)), demonstrating the universality of this electrochemical in-situ doping approach. The XRD pattern of NiFe/Fe-BiVO_4

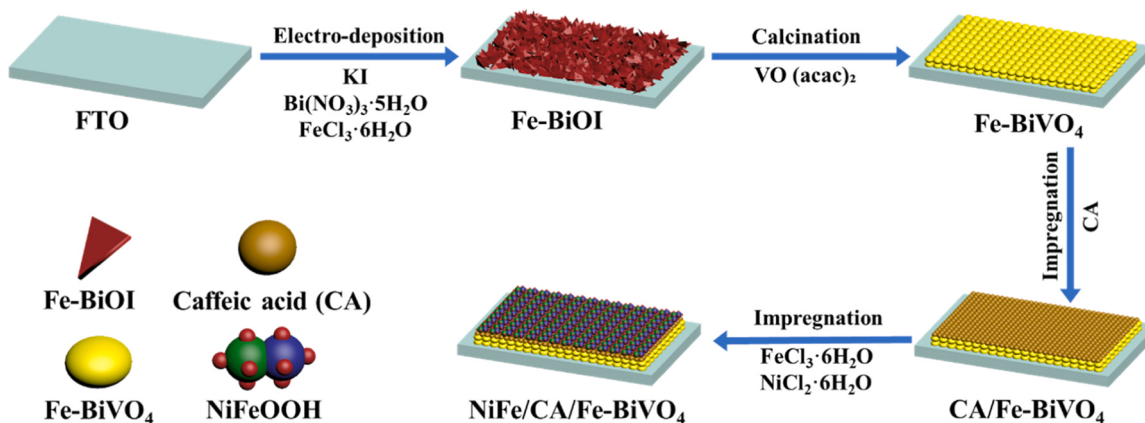


Fig. 1. Schematic illustration for synthesizing NiFe/CA/Fe-BiVO_4 photoanode.

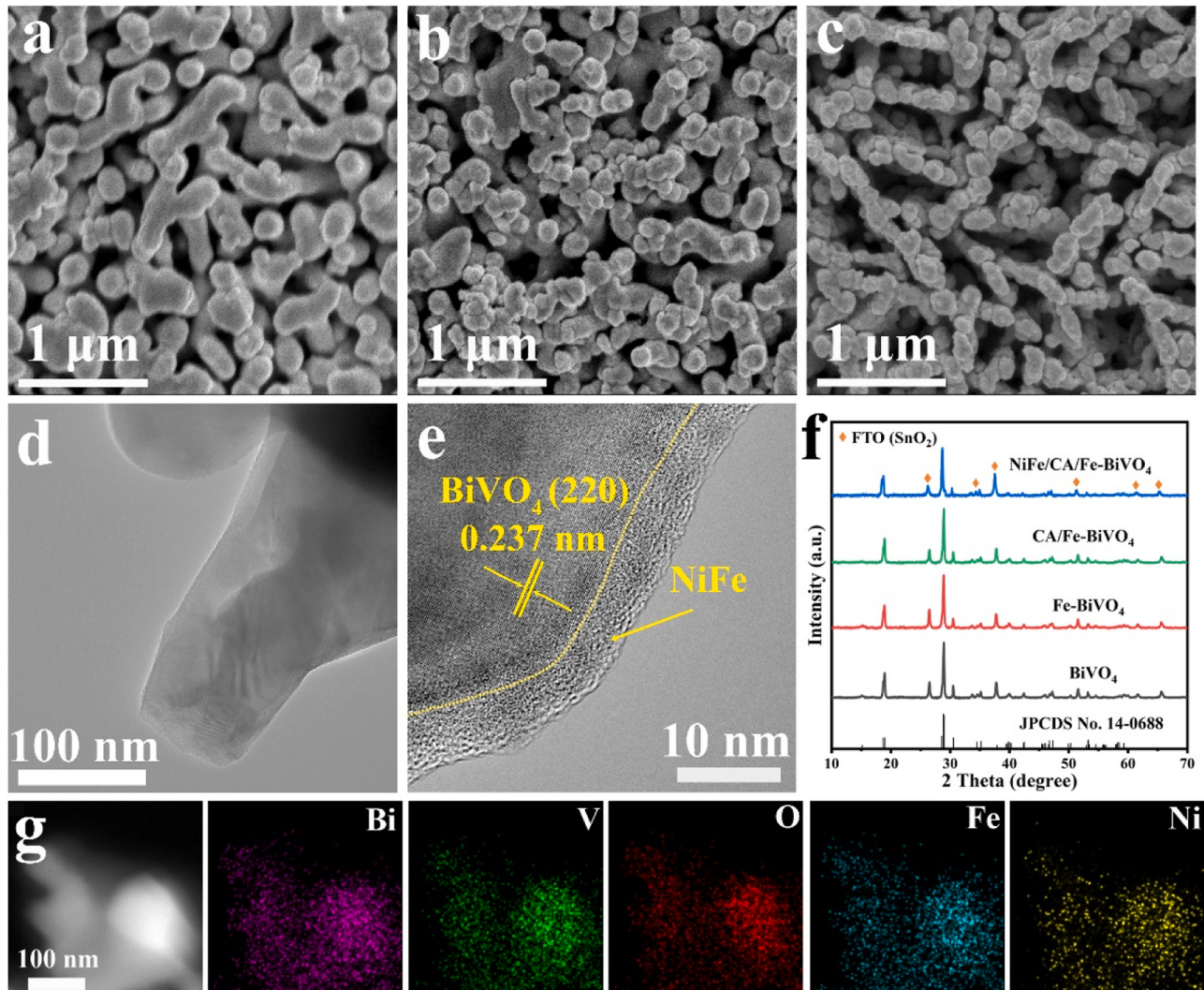


Fig. 2. Characterization of morphology and crystal phase. a), b) and c) SEM images of BiVO₄, Fe-BiVO₄ and NiFe/CA/Fe-BiVO₄. d) TEM and e) HRTEM images of NiFe/CA/Fe-BiVO₄. f) XRD spectra of BiVO₄, Fe-BiVO₄, CA/Fe-BiVO₄ and NiFe/CA/Fe-BiVO₄. g) Elemental mapping images of Bi, V, O and Ni of the NiFe/CA/Fe-BiVO₄ photoanode.

(Fig. S5b) also exhibits no obvious differences with NiFe/CA/Fe-BiVO₄, revealing that the presence of CA has no effect on the crystal phase and crystallinity of the composite photoanode.

Fourier-transform infrared spectroscopy (FTIR) was used to demonstrate the successful anchoring of CA onto BiVO₄ (Fig. 3a). For pure CA, the band at 1670 cm⁻¹ is due to the absorption of C=O, while the band at 950 cm⁻¹ and the weaker bands at 3200–3500 cm⁻¹ are attributed to the out-of-plane bending vibration of the carboxyl group O-H and the outward bending vibration of adjacent hydroxyl groups, respectively [35]. The double bands at around 2800 cm⁻¹ are attributed to the stretching vibration of the C-H bond, which confirms the successful anchoring of CA onto Fe-BiVO₄ and the bridging of NiFeOOH. The solid-state UV-vis spectra of four samples exhibit very similar absorption range (Fig. S6a). Band gap (E_g) values of BiVO₄ and Fe-BiVO₄ catalysts are 2.39 eV and 2.36 eV (Fig. 3b), respectively, through Kubelka-Munk transformation [36].

The Mott-Schottky can be used to determine the conduction band position (E_{CB}) of semiconductors. Both curves of BiVO₄ and Fe-BiVO₄ show positive slopes (Fig. 3c and 3d), suggesting that they are n-type semiconductors [37]. The flat band potentials are 0.18 eV and 0.22 eV for BiVO₄ and Fe-BiVO₄, respectively, and the corresponding E_C positions are -0.02 eV and 0.02 eV. The valence band position (E_{VB}) of BiVO₄ and Fe-BiVO₄ are 2.37 eV and 2.38 eV, respectively, which is

calculated from formula $E_{VB} = E_{CB} + E_g$. Fe doping alters the band structure of BiVO₄ and enhances oxidation capability of Fe-BiVO₄. Furthermore, under the same conditions, the Mott-Schottky curve of Fe-BiVO₄ has a gentler slope compared to BiVO₄, indicating a higher concentration of charge carriers in the composite Fe-BiVO₄ photoanode [37]. This allows for greater extraction of holes from the bulk phase for interfacial reactions, thereby accelerating the separation and transport of photogenerated charge carriers in the bulk phase [37–39].

3.2. Photoelectrochemical performance

All photoelectrochemical tests of the photoanodes were conducted in a 0.5 M borate buffer solution with a three-electrode system (pH = 9.5, AM 1.5 G, 100 mV/cm²). The photocurrent densities of BiVO₄, Fe-BiVO₄, NiFe/Fe-BiVO₄ and NiFe/CA/Fe-BiVO₄ at 1.23 V_{RHE} are 1.5, 4.2, 5.1 and 6.2 mA/cm² (Fig. 4a and S8a), respectively. The relatively poor PEC performance of pure BiVO₄ is mainly attributed to the slow water oxidation kinetics on the surface of BiVO₄ and the recombination of photogenerated charge carriers. Whereas, when Fe was doped in the BiVO₄, the photocurrent density increases to 4.2 mA/cm² for Fe-BiVO₄ at the same voltage. The reason is that more holes are extracted from the bulk phase for surface reactions, thus accelerating the separation and transport of photogenerated charge carriers in the bulk phase and

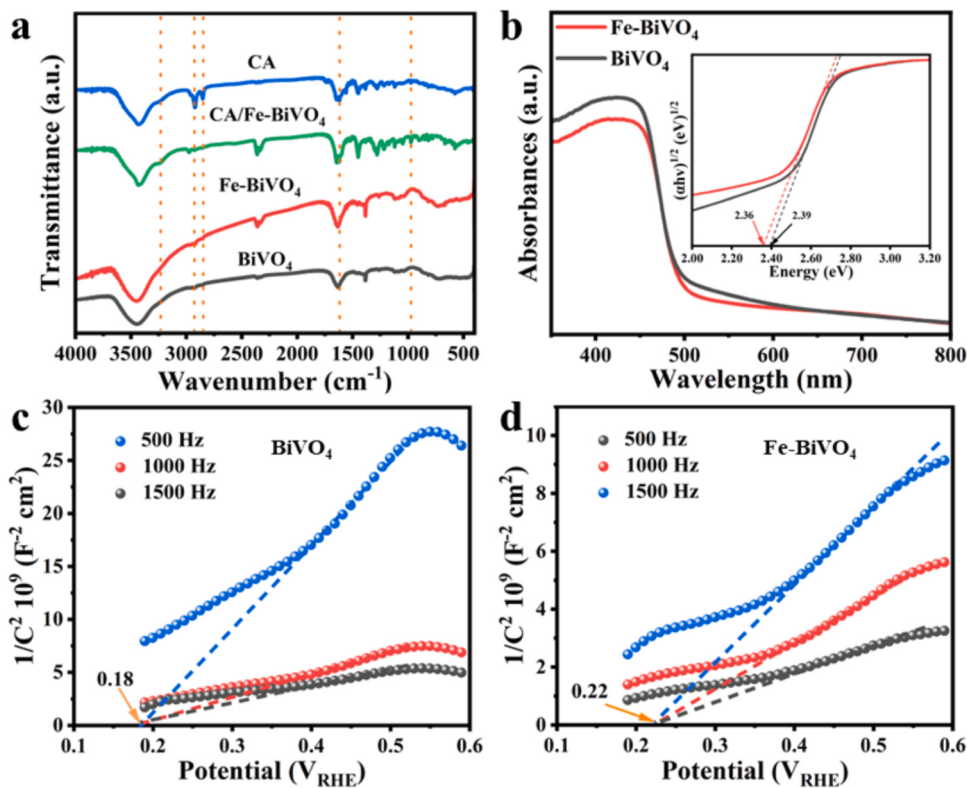


Fig. 3. a) FTIR spectra of BiVO_4 , Fe-BiVO_4 , CA/Fe-BiVO_4 and CA . b) Bandgap calculation diagrams of BiVO_4 and Fe-BiVO_4 . The Mott-Schottky curves of c) BiVO_4 and d) Fe-BiVO_4 .

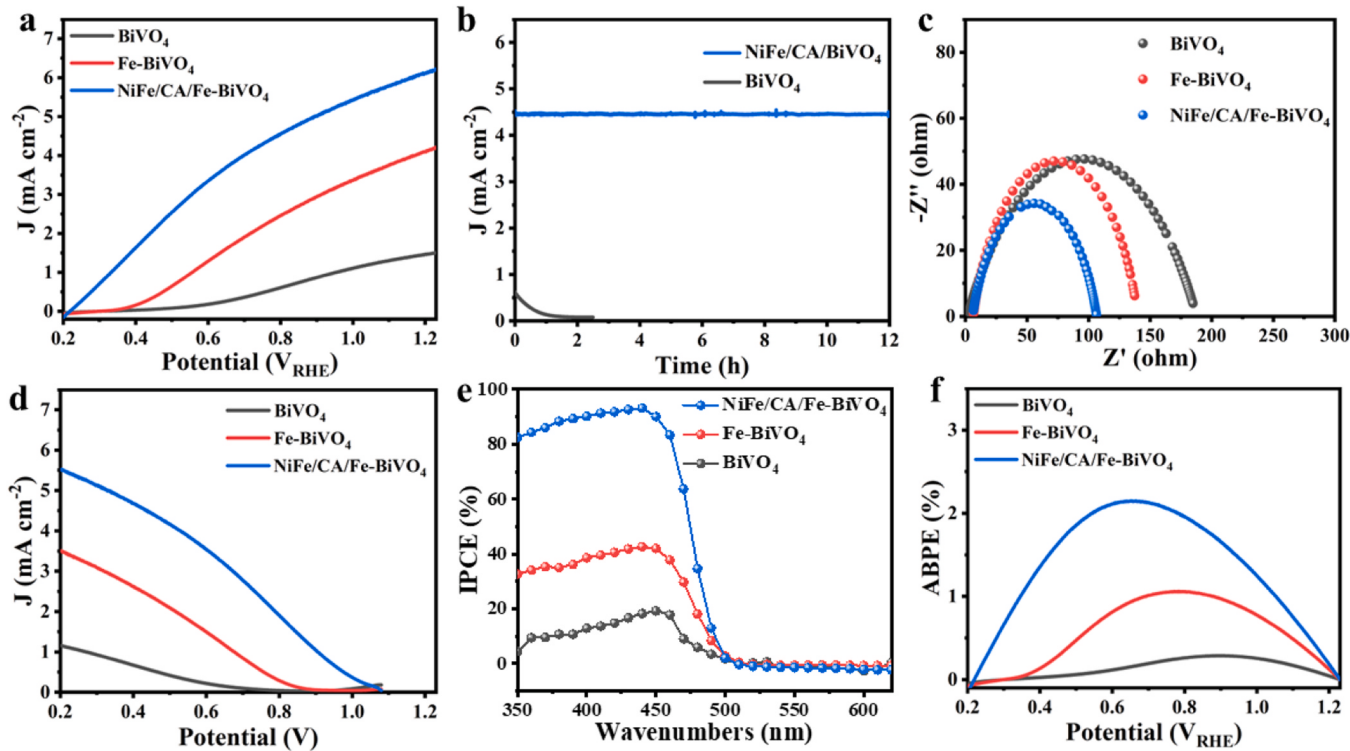


Fig. 4. PEC performance of BiVO_4 , Fe-BiVO_4 and NiFe/CA/Fe-BiVO_4 . a) J - V curves. b) i - t curves of BiVO_4 and NiFe/CA/Fe-BiVO_4 at $0.8 V_{\text{RHE}}$. c) EIS curves. d) Photovoltaic characteristic. e) IPCE curves. f) ABPE curves.

surface. When the Fe-BiVO₄ surface was further modified with a NiFe/CA co-catalyst, the NiFe/CA/Fe-BiVO₄ photoanode exhibits the highest photocurrent density of 6.2 mA/cm² at 1.23 V_{RHE} and more negative onset potential shift, demonstrating excellent PEC performance. NiFe/CA co-catalyst decreases the surface states of BiVO₄ and promotes the transfer of photogenerated carriers between the solid-liquid interfaces.

Stability of photoanode is an important factor to evaluate potential actual application. In addition to its outstanding photoelectrochemical conversion efficiency, the NiFe/CA/Fe-BiVO₄ photoanode also shows improved stability. The photocurrent density of BiVO₄ quickly decays to a very low value under an applied voltage of 0.8 V_{RHE} (Fig. 4b), indicating stability of BiVO₄ is very poor [40]. This is caused by the dissolution of V⁵⁺ from the BiVO₄ crystal into the electrolyte [11,32,40,41]. At high applied bias potential, more accumulated holes causes corresponding changes on the local structure of the BiVO₄, thus destroying the stability of the BiVO₄ lattice and increasing the dissolution of V⁵⁺ on the BiVO₄ surface [11]. However, when strategies of iron doping and NiFe/CA as co-catalyst were adopted, even after 12 hours, the photocurrent density of the NiFe/CA/Fe-BiVO₄ photoanode remains close to its initial value. The presence of the NiFe/CA layer effectively prevents the dissolution of V⁵⁺ from the BiVO₄ photoanode and maintains the stability of the crystal structure.

In order to make clear the interfacial charge transfer and oxygen evolution kinetic, electrochemical impedance spectroscopy (EIS) was measured. The EIS of the photoanodes (Fig. 4c) follows the order of BiVO₄ > Fe-BiVO₄ > NiFe/CA/Fe-BiVO₄. The photoelectric characteristics of the photoanodes can be obtained by subtracting the PEC performance of the photoelectrode from its corresponding electrochemical performance (Fig. 4d). The open-circuit voltage of BiVO₄ is only 0.7 V. After doping with Fe, the open-circuit voltage of Fe-BiVO₄ increases to about 0.85 V. When NiFe/CA layer was further loaded, the open-circuit voltage reaches approximately 1.15 V with short-circuit current density.

To investigate the photogenerated carrier dynamics of oxygen evolution, the incident photon-to-current conversion efficiency (IPCE) values of the photoanodes were tested at 1.23 V_{RHE} in borate buffer.

NiFe/CA/Fe-BiVO₄ exhibits a 93% IPCE value, which is much higher than BiVO₄ (19%) and Fe-BiVO₄ (42%, Fig. 4e), indicating that doping Fe and NiFe/CA co-catalyst layer improve the photon-to-current conversion efficiency of the photoanode. NiFe/CA/Fe-BiVO₄ shows the highest the applied bias photon-to-current efficiency (ABPE) value of 2.15% at 0.65 V_{RHE}, which is much higher than that of Fe-BiVO₄ (1.06% at 0.80 V_{RHE}) and pristine BiVO₄ (0.29% at 0.90 V_{RHE}, Fig. 4f), respectively. These studies demonstrate that the NiFe/CA co-catalyst layer not only significantly improves the PEC performance of the BiVO₄ photoanode but also enhances its stability.

3.3. Spectra and electrochemical analysis

To clarify the interface natures on PEC performance, the charge injection efficiency ($\eta_{\text{injection}}$) and charge separation efficiency ($\eta_{\text{separation}}$) of BiVO₄ and NiFe/CA/Fe-BiVO₄ were evaluated in borate buffer containing Na₂SO₃ as a hole scavenger. The $\eta_{\text{separation}}$ of BiVO₄ is only slightly lower than that of NiFe/CA/Fe-BiVO₄ (Fig. S10). But based on J-V curves (Fig. S8b), the NiFe/CA/Fe-BiVO₄ exhibits a much higher charge injection efficiency ($\eta_{\text{injection}}$) (86.1%) compared with that of BiVO₄ (20.8%, Fig. 5a) at 1.23 V_{RHE}. The NiFe/CA co-catalyst layer significantly contributes to improving charge separation and hole transport at the catalyst-solution interface, and greatly accelerates the surface catalytic reaction rate. After 3 h reaction, the evolution amount of H₂ and O₂ is 353.6 μmol and 160.5 μmol respectively, with an average Faradaic efficiency of 92% (Fig. 5b). This further proves the excellent water oxidation capability of the NiFe/CA/Fe-BiVO₄, which illustrates that the presence of CA is beneficial to the water oxidation reaction occurring on the surface of the NiFe layer.

Charge separation capability was explored in depth by steady-state photoluminescence (PL) spectroscopy. The peak at 473 nm corresponds to the characteristic peak of FTO conductive glass (Fig. 5c). The peak at the wavelength of 490 nm is near the UV-vis absorption edge of BiVO₄, which represents the characteristic absorption peak of BiVO₄ [24, 42, 43]. The appearance of this peak is due to the radiative

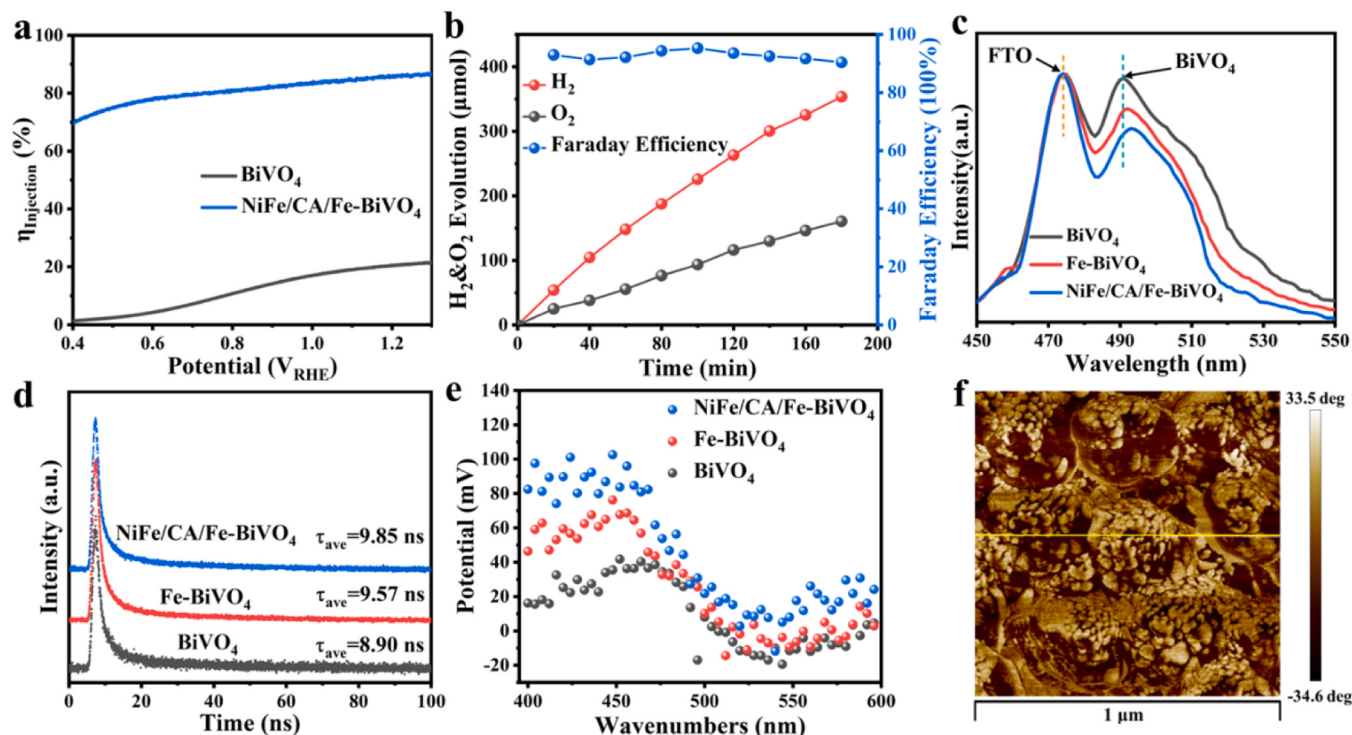


Fig. 5. Spectra and electrochemical analysis. a) Charge injection efficiency curves of BiVO₄ and NiFe/CA/Fe-BiVO₄. b) H₂ and O₂ evolution of NiFe/CA/Fe-BiVO₄. c) PL spectra and d) TR-PL spectra of BiVO₄, Fe-BiVO₄ and NiFe/CA/Fe-BiVO₄. e) SPV spectra of BiVO₄, Fe-BiVO₄ and NiFe/CA/Fe-BiVO₄. f) 2D KPFM spectra of NiFe/CA/Fe-BiVO₄.

recombination of the electrons in V 3d conduction band (CB) and the holes in Bi 6 s and O 2p valence band (VB). The PL peak intensity represent the recombination ability of photogenerated carriers. BiVO₄ photoanode exhibits the strongest PL peak, indicating it has the highest electron-hole recombination ability. However, after doping with Fe and loading with NiFe/CA co-catalyst, the intensity of the PL peak gradually decreases. Fe doping and NiFe/CA co-catalyst both enhance charge separation ability of BiVO₄ photoanode and NiFe/CA/Fe-BiVO₄ gives the strongest charge separation ability. In addition, the PL characteristic peak of Fe-BiVO₄ red shift occurs, which is caused by the narrowing of its bandgap due to Fe doping and oxygen vacancies.

The time-resolved photoluminescence (TR-PL) spectroscopy is used to probe the decay kinetic of photogenerated carrier lifetimes. The average lifetimes of the photogenerated carriers for the BiVO₄, Fe-BiVO₄ and NiFe/CA/Fe-BiVO₄ photoanodes increase successively as 8.90, 9.57 and 9.85 ns (Fig. 5d), fitting parameters shown in Table S2. The tendency is consistent with the photocurrent density and more photogenerated carriers participate in surface reactions. Compared with BiVO₄, the longer photogenerated carrier lifetime of Fe-BiVO₄ disclose doping Fe enhanced charge separation ability. As for NiFe/CA/Fe-BiVO₄, the photogenerated carriers transfer from Fe-BiVO₄ to the NiFe/CA co-catalyst layer, leading to an increase of the photogenerated carrier lifetime. Therefore, NiFe/CA/Fe-BiVO₄ demonstrates the lowest recombination rate of photogenerated carriers, resulting in more photogenerated holes participate in the surface water oxidation.

To further investigate the surface photovoltaic properties, surface photovoltage (SPV) tests were conducted using a Kelvin probe force microscope (KPFM) under illumination. BiVO₄, Fe-BiVO₄ and NiFe/CA/Fe-BiVO₄ all exhibit positive surface photovoltage (Fig. 5e) when they were excited by light with the same wavelength, which is attributed to the enrichment of photogenerated holes at the surface [44]. The surface photovoltage of NiFe/CA/Fe-BiVO₄ is greatly higher than that of Fe-BiVO₄ and BiVO₄, with the differences of approximately 40 mV and 80 mV under 400 nm excitation, respectively. The pronounced surface potential difference elucidates a greater accumulation of photogenerated holes on the NiFe surface in the NiFe/CA/Fe-BiVO₄ composite photoanode, while the photogenerated electrons gather in Fe-BiVO₄. Furthermore, there exists a strong built-in electric field and efficient charge separation between the NiFe/CA co-catalyst and Fe-BiVO₄ photoanode. The two- and three-dimensional images of NiFe/CA/Fe-BiVO₄ (Fig. 5f and S11) obtained from KPFM during the SPV testing show the same morphology as its SEM image (Fig. 2c). Fig. S12 represents the surface roughness analysis at the position indicated by the yellow line in Fig. 5f.

3.4. Active species and electronic states

In order to further confirm the active species during the reaction

process over NiFe/CA/Fe-BiVO₄, electron paramagnetic spectroscopy (EPR) and in-situ Fourier transform infrared (in-situ FTIR) tests were conducted to detect the solution of water oxidation reaction. The generation of superoxide active species ·O₂⁻ during the reaction is verified by the characteristic signal of EPR (Fig. 6a)[45,46]. In the in-situ FTIR spectra, the bands at 1059 and 1160 cm⁻¹ become enhanced with increasing reaction time (Fig. 6b), which are assigned as of O₂^{-*} and OOH^{*} active species[47]. EPR and in-situ FTIR tests disclose that the water molecules adsorbed on the electrode surface are first dissociated into OOH through photogenerated holes on the Fe and Ni active sites under illumination conditions. Then they are transformed into superoxide species (O₂⁻ and ·O₂⁻) intermediates, and further converted into oxygen molecules, which finally are released from the NiFe/CA/Fe-BiVO₄ photoanode surface.

X-ray photoelectron spectroscopy (XPS) was used to investigate the surface chemical states of the photoanode and the electronic states of its elements. Compared with pure BiVO₄, upon doping Fe, the peaks of Bi 4 f, V 2p and O 1 s in Fe-BiVO₄ shift towards lower binding energies (Fig. 7a-c), indicating an increase in electron cloud density around Bi, V and O atoms due to the formation of oxygen vacancies[2,26,48]. When CA was anchored to Fe-BiVO₄ through coordination, the peaks of Bi 4 f, V 2p and O 1 s in CA/Fe-BiVO₄ shift towards higher binding energies, suggesting a strong interaction between CA and Fe-BiVO₄. Subsequently, with the growth of the NiFe co-catalyst layer on CA/Fe-BiVO₄, the peaks of Bi 4 f, V 2p and O 1 s in NiFe/CA/Fe-BiVO₄ shift towards lower binding energies, revealing electron transfer from Fe, Ni to Bi, V atoms [41]. Fe doping and NiFe modification cause the V peak in NiFe/CA/Fe-BiVO₄ to shift towards lower binding energies, which increases the electron cloud density around V atoms, effectively suppressing the dissolution of V⁵⁺ [32,41] and enhancing the stability of the photoanode (Fig. 7b).

The XPS characteristic peaks of BiVO₄ located at 529.9 eV, 531.0 eV and 531.9 eV are attributed to lattice oxygen (O_L), oxygen vacancies (O_V), and adsorbed oxygen (O_{OH}), respectively [49,50] (Fig. 7c and 7d). After doping, the quantity of O_V in Fe-BiVO₄ increases compared to bare BiVO₄, indicating the generation of a certain number of oxygen vacancies. However, when CA was loaded, the quantity of O_V decreases, which is attributed to the anchoring of -OH groups from CA to the oxygen vacancies on the surface of Fe-BiVO₄. In the composite photoanode NiFe/CA/Fe-BiVO₄, both the content of O_V and O_{OH} obviously increase, indicating that the NiFe co-catalyst prepared by the impregnation method contains a large number of O_V and O_{OH} and the NiFe/CA/Fe-BiVO₄ photoanode has better adsorption capacity for water molecules [51,52].

The peaks of Fe 2p_{1/2} (723.9 eV) and Fe 2p_{3/2} (710.9 eV) are attributed to Fe²⁺, while the peaks of Fe 2p_{1/2} (726.4 eV) and Fe 2p_{3/2} (713.0 eV) are attributed to Fe³⁺ (Fig. 7e) [32,50,53]. The peaks of Ni 2p_{3/2} (873.5 eV) and Ni 2p_{1/2} (855.9 eV) with satellite signals are

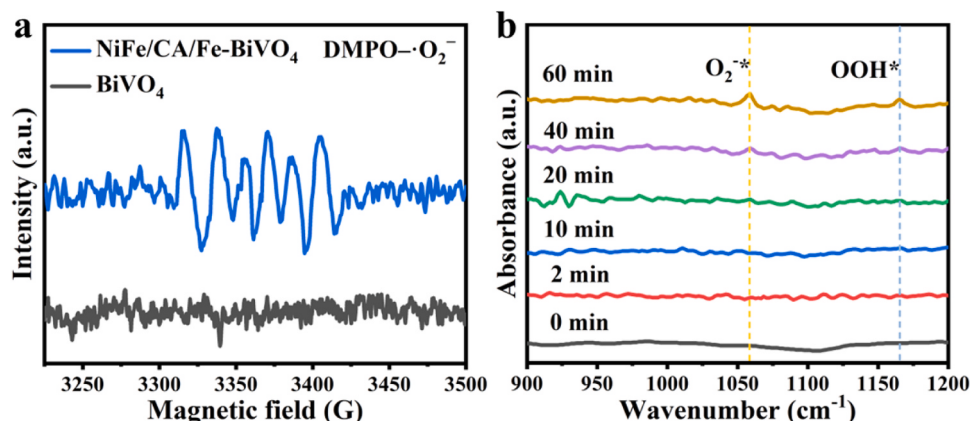


Fig. 6. a) EPR spectra of DMPO-·O₂⁻ in BiVO₄ and NiFe/CA/Fe-BiVO₄ reaction solutions, and b) In-situ FTIR spectra of NiFe/CA/Fe-BiVO₄.

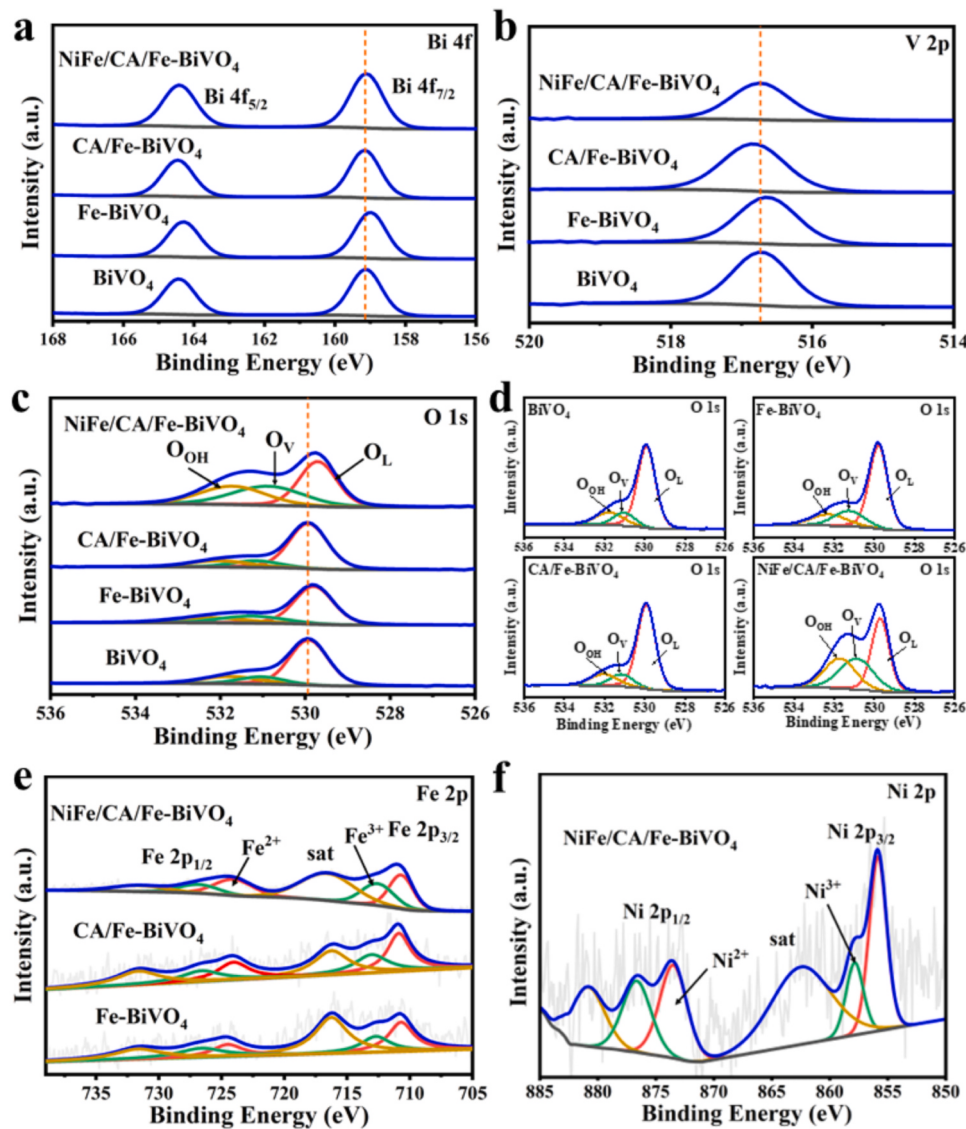


Fig. 7. XPS spectra. a) and b) Bi 4 f and V 2p of BiVO₄, Fe-BiVO₄, CA/Fe-BiVO₄ and NiFe/CA/Fe-BiVO₄. c) and d) O 1 s of BiVO₄, Fe-BiVO₄, CA/Fe-BiVO₄ and NiFe/CA/Fe-BiVO₄. e) Fe 2p of Fe-BiVO₄, CA/Fe-BiVO₄ and NiFe/CA/Fe-BiVO₄. f) Ni 2p of NiFe/CA/Fe-BiVO₄.

attributed to Ni²⁺, while the peaks of Ni 2p_{3/2} (876.6 eV) and Ni 2p_{1/2} (857.8 eV) are attributed to Ni³⁺ (Fig. 7f)[50,54]. After the reaction, the proportion increase of Fe³⁺ and Ni³⁺ (Fig. S13d and S13e) is due to the enrichment of surface holes (Fig. 5e) and the generation of superoxide intermediates (Fig. 6) during the reaction process. Meanwhile, the XPS peak positions of Bi 4 f and V 2p (Fig. S13a and S13b) show nearly no changes. The amounts of O_V and O_{OH} significantly decrease after the reaction (Fig. S13c). XPS proves the proportion change of Ni³⁺, Fe³⁺ and O_V of the NiFe/CA/Fe-BiVO₄ photoanode before and after the reaction. In addition, photocurrent density kept at mostly the initial value after the 12 h stability test at 0.8 V_{RHE}. Based on XPS analysis and stability test, the co-catalyst underwent reconstruction during the reaction. The increase in the proportion of Ni³⁺ and Fe³⁺ enhance their chelating ability with oxygen in water molecules and are the catalytic active sites. Meanwhile, the reduced proportion of O_V improved the stability of the NiFe/CA/Fe-BiVO₄ via regulating the electronic state of the co-catalyst surface.

3.5. DFT calculation and analysis

Furthermore, the density functional theory (DFT) calculation has

been utilized to reveal the changes of electronic states and charge transfer direction. Density of states (DOS) calculations were performed to illustrate the change in electronic states between BiVO₄ and Fe-BiVO₄. Fe-doping generates the Fe impurity states and decreases the bandgap value of BiVO₄ (Fig. 8a and 8b), which is the same as the experimental results. In addition, the replacement of Bi with Fe in BiVO₄ bring about increased density of states near the VB maximum and CB minimum (Fig. 8c and 8d).

In order to clarify the charge transfer direction and separation, the charge density difference calculations were conducted for samples NiFe/CA/Fe-BiVO₄ and NiFe/BiVO₄. Charge redistribution mainly occurred around the NiFe/FeBiVO₄ interface and NiFe/CA interface, and hardly any change was observed in the inner Fe-BiVO₄. The change of charge density at the NiFe/FeBiVO₄ and NiFe/CA interface showed that the electrons mainly transferred from NiFe to Fe-BiVO₄ and CA/BiVO₄ through the interfaces, respectively. Bader charge analysis demonstrates that NiFe co-catalyst donates 0.13 electron to Fe-BiVO₄ for NiFe/Fe-BiVO₄ (Fig. 8e). While for sample of NiFe/CA/Fe-BiVO₄, the number of 0.25 electrons are transferred from NiFe to CA/Fe-BiVO₄ (Fig. 8f). The calculation results illustrate that CA facilitates electron transport from co-catalyst NiFe to Fe-BiVO₄, which enhances interfacial polarization,

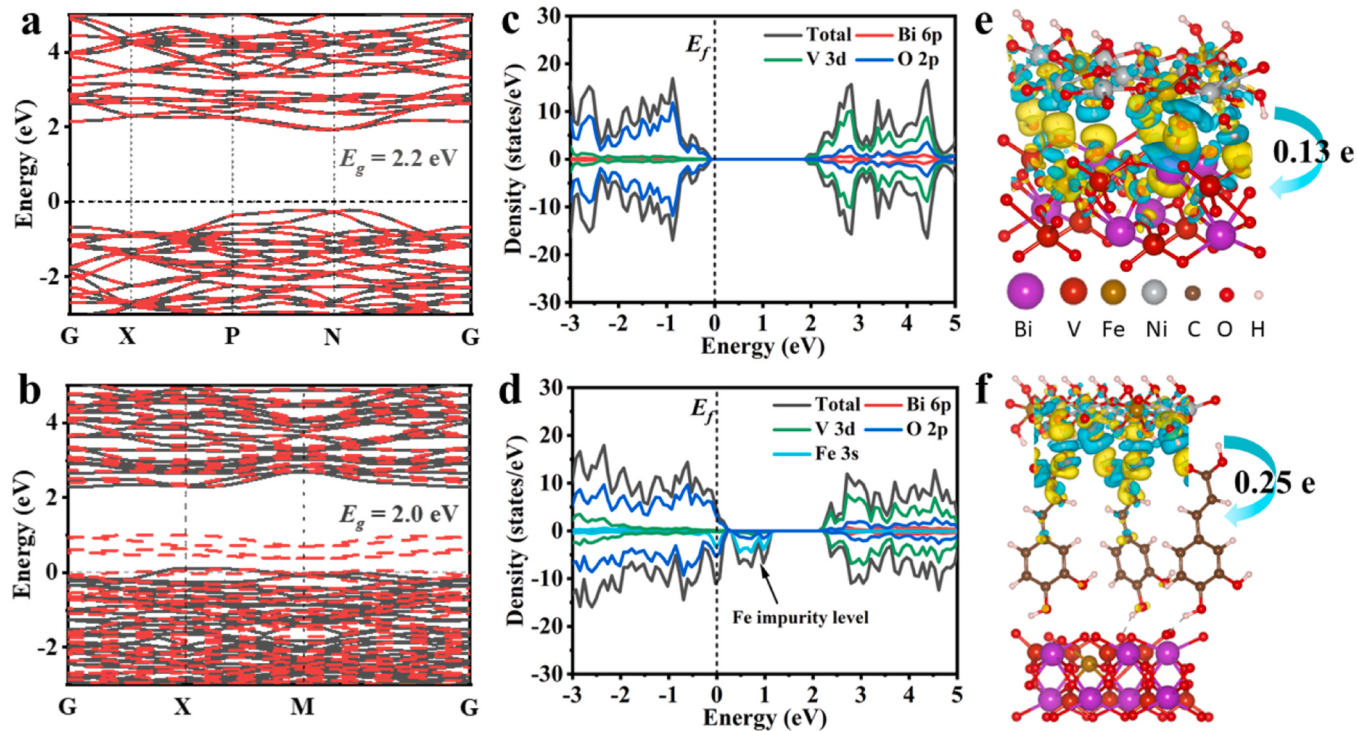


Fig. 8. DFT calculation. a) and b) The calculated electron energy bands of BiVO₄ and Fe-BiVO₄. c) and d) DOS of BiVO₄ and Fe-BiVO₄. e) and f) Charge density difference of NiFe/Fe-BiVO₄ and NiFe/CA/Fe-BiVO₄.

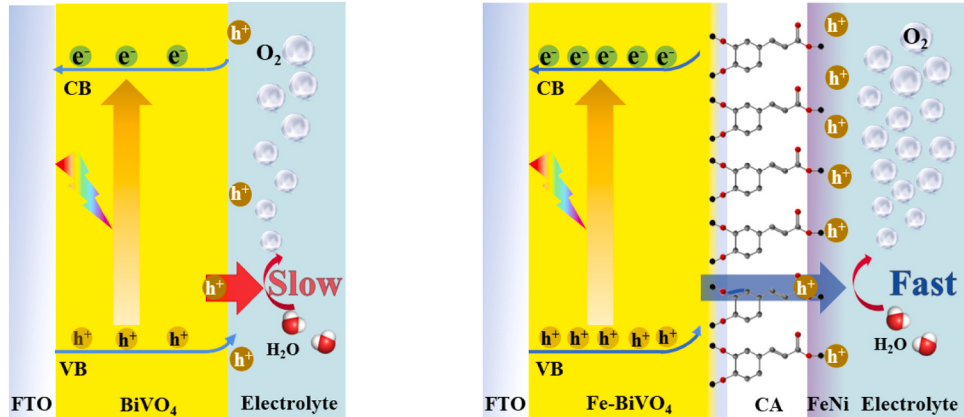


Fig. 9. Schematic illustration of charge transfer and water oxidation of NiFe/CA/Fe-BiVO₄ photoelectrode.

inter-interfacial coupling and electronic state modulation, thus effectively inhibiting the recombination of photogenerated carriers.

Based on the results mentioned above, the photoelectrochemical water oxidation and charge transfer of NiFe/CA/Fe-BiVO₄ are illustrated in Fig. 9. Due to the strong interfacial interaction between the Fe-BiVO₄ photoanode and the NiFe co-catalyst, photogenerated holes can rapidly migrate to the catalyst surface, while photogenerated electrons quickly transfer to the counter electrode through the external circuit, significantly facilitating charge separation and transfer. By anchoring the CA bridge connection layer, the surface states of Fe-BiVO₄ are effectively passivated, controlling the electron states and enhancing the strong interfacial coupling between the Fe-BiVO₄ and NiFe co-catalyst. Therefore, the recombination of photogenerated charge carriers is effectively suppressed and electron transfer from the NiFe co-catalyst layer to Fe-BiVO₄ is efficiently promoted.

4. Conclusion

In summary, we developed a novel photoanode synthesis method for PEC water oxidation through combination doping and co-catalyst strategy. First, uniform Fe doped BiVO₄ was obtained by in-situ electrochemical doping and calcination. Subsequently, a hybrid NiFe/CA/Fe-BiVO₄ photoanode was fabricated by sequential deposition of caffeic acid (CA) as bridging reagent and NiFeOOH (NiFe) as co-catalyst to Fe-BiVO₄ through self-assembly. Under illumination with an applied bias of 1.23 V_{RHE} (AM 1.5 G, 100 mV/cm²), the photocurrent density reached 6.2 mA/cm², accompanied with an ABPE of 2.15% at 0.65 V_{RHE} for the PEC water oxidation reaction. Photoelectrochemical performance remained nearly the initial photocurrent density after 12 hours at 0.8 V_{RHE}. Systematical characterizations revealed that the good PEC performance of the NiFe/CA/Fe-BiVO₄ photoanode could be attributed to the simultaneous improvement in separation of photogenerated charge carriers and interfacial OER catalytic kinetics, which is resulted

from the synergetic effect between the Fe and Ni in the co-catalyst of NiFeOOH. In addition, EPR and in-situ FTIR confirm the generation of superoxide active species (O_2 and $\cdot O_2$) during the PEC water oxidation reaction. This work provides a new strategy for designing highly efficient composite photoanodes for PEC.

CRediT authorship contribution statement

Xiaohu Li: Writing – original draft, Investigation, Formal analysis, Data curation. **Junhao Wu:** Software, Formal analysis. **Congzhao Dong:** Methodology, Investigation. **Yao Kou:** Data curation. **Chunlian Hu:** Validation, Formal analysis. **Jinnuo Zang:** Investigation. **Jiayu Zhu:** Methodology, Investigation. **Baochun Ma:** Resources. **Yuanyuan Li:** Resources, Software. **Yong Ding:** Writing – original draft, Supervision, Project administration, Funding acquisition.

Declaration of Competing Interest

The authors declare that they have no known competing financial interests or personal relationships that could have appeared to influence the work reported in this paper.

Data Availability

Data will be made available on request.

Acknowledgements

This work was financially supported by the National Natural Science Foundation of China (22075119) and the Natural Science Foundation of Gansu Province (21JR7RA440).

Supporting Information

Supplementary data associated with this article can be found in the online version.

Appendix A. Supporting information

Supplementary data associated with this article can be found in the online version at [doi:10.1016/j.apcatb.2024.124096](https://doi.org/10.1016/j.apcatb.2024.124096).

References

- [1] S. Wang, G. Liu, L. Wang, Crystal facet engineering of photoelectrodes for photoelectrochemical water splitting, *Chem. Rev.* 119 (2019) 5192–5247.
- [2] J.B. Pan, B.H. Wang, J.B. Wang, H.Z. Ding, W. Zhou, X. Liu, J.R. Zhang, S. Shen, J. K. Guo, L. Chen, C.-T. Au, L.-L. Jiang, S.-F. Yin, Activity and stability boosting of an oxygen-vacancy-rich BiVO₄ photoanode by NiFe-MOFs thin layer for water oxidation, *Angew. Chem. Int. Ed.* 60 (2021) 1433–1440.
- [3] J. Ma, H. Chi, A. Wang, P. Wang, H. Jing, T. Yao, C. Li, Identifying and removing the interfacial states in metal-oxide-semiconductor schottky si photoanodes for the highest fill factor, *J. Am. Chem. Soc.* 144 (2022) 17540–17548.
- [4] B. Zhang, L. Wang, Y. Zhang, Y. Ding, Y. Bi, Ultrathin FeOOH nanolayers with abundant oxygen vacancies on BiVO₄ photoanodes for efficient water oxidation, *Angew. Chem. Int. Ed.* 57 (2018) 2248–2252.
- [5] Y. Lu, Y. Yang, X. Fan, Y. Li, D. Zhou, B. Cai, L. Wang, K. Fan, K. Zhang, Boosting charge transport in BiVO₄ photoanode for solar water oxidation, *Adv. Mater.* 34 (2022) 210178.
- [6] Q. Zhang, M. Liu, W. Zhou, Y. Zhang, W. Hao, Y. Kuang, H. Liu, D. Wang, L. Liu, J. Ye, A novel Cl-modification approach to develop highly efficient photocatalytic oxygen evolution over BiVO₄ with AQE of 34.6%, *Nano Energy* 81 (2021) 105651.
- [7] Y. Deng, X. Fu, Y. Zhang, Y. Zhu, Y. Wei, Efficient oxygen evolution reaction on polyethylene glycol-modified BiVO₄ photoanode by speeding up proton transfer, *Small* 18 (2022) 2201410.
- [8] T.W. Kim, K.-S. Choi, Nanoporous BiVO₄ photoanodes with dual-layer oxygen evolution catalysts for solar water splitting, *Science* 343 (2014) 990–994.
- [9] Q. Meng, B. Zhang, L. Fan, H. Liu, M. Valvo, K. Edström, M. Cuartero, R. De Marco, G.A. Crespo, L. Sun, Efficient BiVO₄ photoanodes by postsynthetic treatment: remarkable improvements in photoelectrochemical performance from facile borate modification, *Angew. Chem. Int. Ed.* 131 (2019) 19203–19209.
- [10] B. Liu, X. Wang, Y. Zhang, L. Xu, T. Wang, X. Xiao, S. Wang, L. Wang, W. Huang, A BiVO₄ photoanode with a VO_x layer bearing oxygen vacancies offers improved charge transfer and oxygen evolution kinetics in photoelectrochemical water splitting, *Angew. Chem. Int. Ed.* 62 (2023) e202217346.
- [11] D.K. Lee, K.-S. Choi, Enhancing long-term photostability of BiVO₄ photoanodes for solar water splitting by tuning electrolyte composition, *Nat. Energy* 3 (2018) 53–60.
- [12] J. Su, L. Guo, N. Bao, C.A. Grimes, Nanostructured WO₃/BiVO₄ heterojunction films for efficient photoelectrochemical water splitting, *Nano Lett.* 11 (2011) 1928–1933.
- [13] M.-W. Kim, E. Samuel, K. Kim, H. Yoon, B. Joshi, M.T. Swihart, S.S. Yoon, Tuning the morphology of electrosprayed BiVO₄ from nanopillars to nanoferns via pH control for solar water splitting, *J. Alloy. Compd.* 769 (2018) 193–200.
- [14] M. Lamers, W. Li, M. Favaro, D.E. Starr, D. Friedrich, S. Lardhi, L. Cavallo, M. Harb, R. van de Krol, L.H. Wong, Enhanced carrier transport and bandgap reduction in sulfur-modified BiVO₄ photoanodes, *Chem. Mater.* 30 (2018) 8630–8638.
- [15] H. Lu, V. Andrei, K.J. Jenkinson, A. Regoutz, N. Li, C.E. Creissen, A.E. Wheatley, H. Hao, E. Reisner, D.S. Wright, Single-source bismuth (transition metal) polyoxovanadate precursors for the scalable synthesis of doped BiVO₄ photoanodes, *Adv. Mater.* 30 (2018) 1804033.
- [16] P. Stathi, M. Solakidou, Y. Deligiannakis, Lattice defects engineering in W-, Zr-doped BiVO₄ by flame spray pyrolysis: enhancing photocatalytic O₂ evolution, *Nanomaterials* 11 (2021) 501.
- [17] C.W. Kim, Y.S. Son, M.J. Kang, D.Y. Kim, Y.S. Kang, (040)-crystal facet engineering of BiVO₄ plate photoanodes for solar fuel production, *Adv. Energy Mater.* 6 (2016) 1501754.
- [18] H.S. Han, S. Shin, D.H. Kim, I.J. Park, J.S. Kim, P.-S. Huang, J.-K. Lee, I.S. Cho, X. Zheng, Boosting the solar water oxidation performance of a BiVO₄ photoanode by crystallographic orientation control, *Energy Environ. Sci.* 11 (2018) 1299–1306.
- [19] D. Li, Y. Liu, W. Shi, C. Shao, S. Wang, C. Ding, T. Liu, F. Fan, J. Shi, C. Li, Crystallographic-orientation-dependent charge separation of BiVO₄ for solar water oxidation, *ACS Energy Lett.* 4 (2019) 825–831.
- [20] K.-H. Ye, H. Li, D. Huang, S. Xiao, W. Qiu, M. Li, Y. Hu, W. Mai, H. Ji, S. Yang, Enhancing photoelectrochemical water splitting by combining work function tuning and heterojunction engineering, *Nat. Commun.* 10 (2019) 3687.
- [21] K. Zhang, B. Jin, C. Park, Y. Cho, X. Song, X. Shi, S. Zhang, W. Kim, H. Zeng, J. H. Park, Black phosphorene as a hole extraction layer boosting solar water splitting of oxygen evolution catalysts, *Nat. Commun.* 10 (2019) 2001.
- [22] Y. Song, X. Zhang, Y. Zhang, P. Zhai, Z. Li, D. Jin, J. Cao, C. Wang, B. Zhang, J. Gao, L. Sun, J. Hou, Engineering MoO_x/MXene hole transfer layers for unexpected boosting of photoelectrochemical water oxidation, *Angew. Chem. Int. Ed.* 61 (2022) e202200946.
- [23] Y. Shi, Y. Yu, Y. Yu, Y. Huang, B. Zhao, B. Zhang, Boosting photoelectrochemical water oxidation activity and stability of Mo-doped BiVO₄ through the uniform assembly coating of NiFe-phenolic networks, *ACS Energy Lett.* 3 (2018) 1648–1654.
- [24] B. Zhang, S. Yu, Y. Dai, X. Huang, L. Chou, G. Lu, G. Dong, Y. Bi, Nitrogen-incorporation activates NiFeO_x catalysts for efficiently boosting oxygen evolution activity and stability of BiVO₄ photoanodes, *Nat. Commun.* 12 (2021) 6969.
- [25] D.K. Zhong, S. Choi, D.R. Gamelin, Near-complete suppression of surface recombination in solar photoelectrolysis by “Co-PI” catalyst-modified W:BiVO₄, *J. Am. Chem. Soc.* 133 (2011) 18370–18377.
- [26] T.W. Kim, Y. Ping, G.A. Galli, K.-S. Choi, Simultaneous enhancements in photon absorption and charge transport of bismuth vanadate photoanodes for solar water splitting, *Nat. Commun.* 6 (2015) 8769.
- [27] M. Rohloff, B. Anke, S. Zhang, U. Gernert, C. Scheu, M. Lerch, A. Fischer, Mo-doped BiVO₄ thin films-high photoelectrochemical water splitting performance achieved by a tailored structure and morphology, *Sustain. Energy Fuels* 1 (2017) 1830–1846.
- [28] M. Rohloff, B.R. Anke, O. Kasian, S. Zhang, M. Lerch, C. Scheu, A. Fischer, Enhanced photoelectrochemical water oxidation performance by fluorine incorporation in BiVO₄ and Mo:BiVO₄ thin film photoanodes, *ACS Appl. Mater. Interfaces* 11 (2019) 16430–16442.
- [29] A. Ngoipala, L. Ngamwongwan, I. Fongkaew, S. Junghawan, P. Hirunsit, S. Limpijumpong, S. Suthirakun, On the enhanced reducibility and charge transport properties of phosphorus-doped BiVO₄ as photocatalysts: a computational study, *J. Phys. Chem. C* 124 (2020) 4352–4362.
- [30] Y. Kuang, Q. Jia, H. Nishiyama, T. Yamada, A. Kudo, K. Domen, A front-illuminated nanostructured transparent BiVO₄ photoanode for >2% efficient water splitting, *Adv. Energy Mater.* 6 (2016) 1501645.
- [31] R.-T. Gao, D. He, L. Wu, K. Hu, X. Liu, Y. Su, L. Wang, Towards long-term photostability of nickel hydroxide/BiVO₄ photoanodes for oxygen evolution catalysts via in situ catalyst tuning, *Angew. Chem. Int. Ed.* 132 (2020) 6272–6277.
- [32] Z. Zhang, X. Huang, B. Zhang, Y. Bi, High-performance and stable BiVO₄ photoanodes for solar water splitting via phosphorus-oxygen bonded FeNi catalysts, *Energy Environ. Sci.* 15 (2022) 2867–2873.
- [33] S. Feng, T. Wang, B. Liu, C. Hu, L. Li, Z.-J. Zhao, J. Gong, Enriched surface oxygen vacancies of photoanodes by photoetching with enhanced charge separation, *Angew. Chem. Int. Ed.* 132 (2020) 2060–2064.
- [34] K.J. McDonald, K.-S. Choi, A new electrochemical synthesis route for a BiOI electrode and its conversion to a highly efficient porous BiVO₄ photoanode for solar water oxidation, *Energy Environ. Sci.* 5 (2012) 8553–8557.
- [35] P. Xu, H. Uyama, J.E. Whitten, S. Kobayashi, D.L. Kaplan, Peroxidase-catalyzed in situ polymerization of surface orientated caffeic acid, *J. Am. Chem. Soc.* 127 (2005) 11745–11753.

- [36] H.-Y. Jiang, P. Li, J. Ye, J. Lin, Synthesis and photocatalytic properties of metastable β -Bi₂O₃ stabilized by surface-coordination effects, *J. Mater. Chem. A* 3 (2015) 5119–5125.
- [37] X. Cao, C. Xu, X. Liang, J. Ma, M. Yue, Y. Ding, Rationally designed/assembled hybrid BiVO₄-based photoanode for enhanced photoelectrochemical performance, *Appl. Catal. B* 260 (2020) 118136.
- [38] G. Wang, Y. Ling, D.A. Wheeler, K.E. George, K. Horsley, C. Heske, J.Z. Zhang, Y. Li, Facile synthesis of highly photoactive α -Fe₂O₃-based films for water oxidation, *Nano Lett.* 11 (2011) 3503–3509.
- [39] F. Ning, M. Shao, S. Xu, Y. Fu, R. Zhang, M. Wei, D.G. Evans, X. Duan, TiO₂/graphene/NiFe-layered double hydroxide nanorod array photoanodes for efficient photoelectrochemical water splitting, *Energy Environ. Sci.* 9 (2016) 2633–2643.
- [40] Y. Kuang, Q. Jia, G. Ma, T. Hisatomi, T. Minegishi, H. Nishiyama, M. Nakabayashi, N. Shibata, T. Yamada, A. Kudo, Ultrastable low-bias water splitting photoanodes via photocorrosion inhibition and in situ catalyst regeneration, *Nat. Energy* 2 (1) (2016) 9.
- [41] B. Zhang, X. Huang, Y. Zhang, G. Lu, L. Chou, Y. Bi, Unveiling the activity and stability origin of BiVO₄ photoanodes with FeNi oxyhydroxides for oxygen evolution, *Angew. Chem. Int. Ed.* 59 (2020) 18990–18995.
- [42] A. Kudo, K. Omori, H. Kato, A novel aqueous process for preparation of crystal form-controlled and highly crystalline BiVO₄ powder from layered vanadates at room temperature and its photocatalytic and photophysical properties, *J. Am. Chem. Soc.* 121 (1999) 11459–11467.
- [43] S. Gu, W. Li, F. Wang, S. Wang, H. Zhou, H. Li, Synthesis of buckhorn-like BiVO₄ with a shell of CeO_x nanodots: effect of heterojunction structure on the enhancement of photocatalytic activity, *Appl. Catal. B* 170 (2015) 186–194.
- [44] J. Zhu, F. Fan, R. Chen, H. An, Z. Feng, C. Li, Direct imaging of highly anisotropic photogenerated charge separations on different facets of a single BiVO₄ photocatalyst, *Angew. Chem. Int. Ed.* 127 (2015) 9239–9242.
- [45] F. Lin, D. Wang, Z. Jiang, Y. Ma, J. Li, R. Li, C. Li, Photocatalytic oxidation of thiophene on BiVO₄ with dual co-catalysts Pt and RuO₂ under visible light irradiation using molecular oxygen as oxidant, *Energy Environ. Sci.* 5 (2012) 6400–6406.
- [46] Q. Hu, Y. Dong, K. Ma, X. Meng, Y. Ding, Amidation crosslinking of polymeric carbon nitride for boosting photocatalytic hydrogen peroxide production, *J. Catal.* 413 (2022) 321–330.
- [47] Y. Lin, L. Yu, L. Tang, F. Song, R. Schloegl, S. Heumann, In situ identification and time-resolved observation of the interfacial state and reactive intermediates on a cobalt oxide nanocatalyst for the oxygen evolution reaction, *ACS Catal.* 12 (2022) 5345–5355.
- [48] S. Wang, P. Chen, J.H. Yun, Y. Hu, L. Wang, An electrochemically treated BiVO₄ photoanode for efficient photoelectrochemical water splitting, *Angew. Chem. Int. Ed.* 129 (2017) 8620–8624.
- [49] S. Wang, T. He, P. Chen, A. Du, K. Ostrikov, W. Huang, L. Wang, In situ formation of oxygen vacancies achieving near-complete charge separation in planar BiVO₄ photoanodes, *Adv. Mater.* 32 (2020) 2001385.
- [50] J. Lin, X. Han, S. Liu, Y. Lv, X. Li, Y. Zhao, Y. Li, L. Wang, S. Zhu, Nitrogen-doped cobalt-iron oxide cocatalyst boosting photoelectrochemical water splitting of BiVO₄ photoanodes, *Appl. Catal. B* 320 (2023) 121947.
- [51] C. Kim, S.O. Park, S.K. Kwak, Z. Xia, G. Kim, L. Dai, Concurrent oxygen reduction and water oxidation at high ionic strength for scalable electrosynthesis of hydrogen peroxide, *Nat. Commun.* 14 (2023) 5822.
- [52] X. Zhao, J. Wang, L. Lian, G. Zhang, P. An, K. Zeng, H. He, T. Yuan, J. Huang, L. Wang, Oxygen vacancy-reinforced water-assisted proton hopping for enhanced catalytic hydrogenation, *ACS Catal.* 13 (2023) 2326–2334.
- [53] F.N.I. Sari, H.-S. Chen, A. Kumar Anbalagan, Y.-J. Huang, S.-C. Haw, J.-M. Chen, C.-H. Lee, Y.-H. Su, J.-M. Ting, V-doped, divacancy-containing β -FeOOH electrocatalyst for high performance oxygen evolution reaction, *Chem. Eng. J.* 438 (2022) 135515.
- [54] M. Cai, Q. Zhu, X. Wang, Z. Shao, L. Yao, H. Zeng, X. Wu, J. Chen, K. Huang, S. Feng, Formation and stabilization of NiOOH by introducing α -FeOOH in LDH: composite electrocatalyst for oxygen evolution and urea oxidation reactions, *Adv. Mater.* 35 (2023) 2209338.